COMPDYN 2011
ECCOMAS Thematic Conference on
Computational Methods in Structural Dynamics and Earthquake Engineering
M. Papadrakakis, M. Fragiadakis, V. Plevris (eds.)
Corfu, Greece, 25-28 May 2011

REFLECTION OF PLANE HARMONIC WAVES AT A PLANE INTERFACE OF A SEMI-INFINITE LATTICE AND A SEMI-INFINITE CONTINUUM

Asiya M. Kudarova[1], **Andrei V. Metrikine**[2]

[1]Institute for Problems in Mechanical Engineering RAS
Bolshoy pr. V.O. 61, St. Petersburg, 199178, Russia
e-mail: asya.kudarova@gmail.com

[2] Delft University of Technology
Faculty of Civil Engineering and GeoSciences, P.O. Box 5048, 2600 GA, The Netherlands
e-mail: A.Metrikine@tudelft.nl

Keywords: wave reflection, dynamic coupling, discrete lattice, elastic continuum

Abstract. *Whereas the wave reflection and refraction at an interface of two continua has been studied in detail and has become a matter of text books, the wave reflection at an interface of a lattice and a continuum does not seem to have been systematically studied. The aim of this development is to close this gap. Two semi-infinite elastic media are considered in contact at a plane interface. One of these media is modelled using a rectangular network of identical masses and springs (hereafter called a lattice), whereas the other one is described by the equations of the classical elastic continuum. The wave reflection at the interface with the classical continuum is studied assuming that a plane harmonic wave falls from the lattice on the interface. The reflection coefficients for the reflected compressional and shear waves are found as functions of the wave frequency and of the incidence angle. It is shown that the reflection at low frequencies can be made very small by properly choosing the parameters of the continuum. However, the reflection coefficients inevitably grow with increase of the frequency and can reach the values close to one. This is to be expected as the classical continuum is capable of approximating a lattice only at relatively low frequencies.*

1 INTRODUCTION

The dynamic coupling of the discrete and continuum domains is widely used in concurrent multiscale simulations. The aim of such a coupling is to decrease the calculation time. This is achieved by breaking the computational domain into two parts. In the main part, where a detailed modeling is necessary, a discrete model is adopted. The rest of the domain is assumed to be occupied by a corresponding continuum. Often the role of this continuum is simply to serve as non-reflecting boundary or to pass the reflections from the outer boundaries of the computational domain. In either case the wave reflection from the fictitious boundary between the discrete and continuum domains should be minimized. This is the challenge researches are trying to cope with. A number of approaches have been introduced to couple discrete and continuum representations of materials. A coarse-grained molecular dynamics (CGMD) method has been proposed by Rudd and Broughton [3], an approach based on the Green's functions formalism has been proposed in [4] – [5] to derive the non-reflecting boundary conditions. E [6] and his co-workers contributed on the study of optimal matching conditions, Wagner and Liu introduced the bridging scale decomposition (BSL) method [7] which was developed further by Xiao and Belytschko [8]. However, most of the methods either have limitations in their application or are often too complicated to implement. Moreover, in most approaches the wave reflections either have not been yet properly studied in multidimensional cases or the non-reflecting boundary conditions have been introduced only for 1D case.

In this development a systematic investigation into the wave reflection at the interface of a square lattice composed of masses and springs and a classical isotropic continuum is presented. The parameters of the lattice are chosen such as to assure that in the long-wave approximation the lattice is reduced to the continuum, with which it is coupled. The main aim of this investigation is to demonstrate the poor ability of the classical continuum to absorb high-frequency waves in the lattice. Such demonstration is necessary to motivate the use of generalized continua at the discrete-continuum interfaces. The promising character of the latter approach has recently been demonstrated in [9], where it has been shown that the reflections from the boundary between the 1D chain of masses and springs and a gradient continuum of the second order can be eliminated at the entire frequency band.

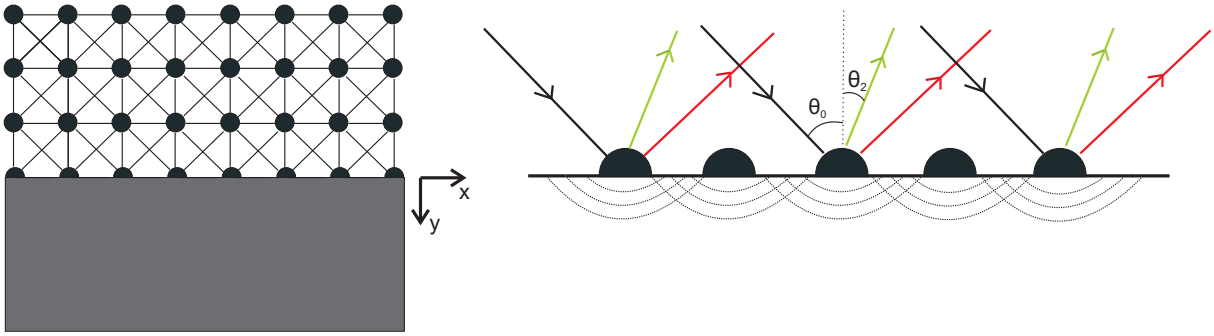

Figure 1: Coupled discrete and continuum domains (left) and wave reflection and transmission at the interface (right).

Two elastic semi-infinite half-spaces in contact are considered in this paper (see Figure 1). One of the half-spaces is described by the equations of motion of the classical continuum and another one is modelled using the system of masses and translational springs that form a so-called square lattice. It is assumed that the plane harmonic wave, either longitudinal or transversal

one, propagates in the lattice towards the interface between two domains. The energy of the reflected longitudinal and transversal waves is studied as a function of the frequency and the angle of incidence θ_0 in terms of the energy reflection coefficient.

The paper is organized as follows. First, the governing equations for the lattice and the correspondence between the parameters of the lattice and of the continuum in the long-wave limit are introduced. Thereafter the propagation characteristics of the body waves in the lattice are derived. The following boundary conditions are introduced: the continuity of forces and displacements at the interface. Then the equations of motion of the continuum are solved with the certain boundary conditions and the displacements in the continuum in the form of integrals are derived. Then the integrals for the displacements at the interface are evaluated. The system of boundary conditions is applied to find the amplitudes of the reflected waves. Then the energy reflection coefficients are introduced. Finally, the results and conclusions are presented.

2 GOVERNING EQUATIONS FOR THE LATTICE

The inner cell of the square lattice consists of identical masses M and translational springs: axial κ_{axi} and diagonal κ_{dia}. The derivation of the equations of motion for the square lattice with translational and shear springs can be found in [1]. It is assumed that the dynamic behaviour of the lattice corresponds to that of the isotropic classical elastic continuum in the long-wave limit. This assumption requires the following relations between the parameters of the lattice and of the continuum [1]:

$$M = \rho d^2 h, \quad \kappa_{axi} = 2\kappa_{dia}, \quad \kappa_{dia} = h\mu, \quad 2\kappa_{dia} = h(\lambda + \mu), \tag{1}$$

where ρ is the mass density of the continuum, λ and μ are Lame's constants of the elastic continuum, d is the inter-particle distance in the lattice along the axes, h is a parameter of length in the direction normal to the $[x, y]$ plane. The introduction of this parameter is required to couple the 2D-lattice with the 3D-continuum. It follows from the equalities (1) that $\lambda = \mu$ in the continuum that corresponds to such a lattice in the long-wave limit.

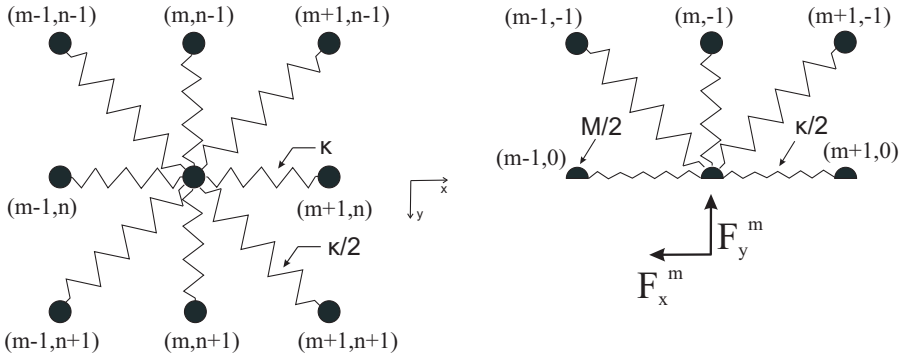

Figure 2: Inner (left) and boundary (right) cells of the lattice.

We denote $\kappa = \kappa_{axi} = 2\kappa_{dia}$. Then the equations of motion for the inner cell of the lattice (depicted in the left part of Figure 2) read

$$M\mathrm{d}_{tt}u_x^{(m,n)} = \kappa/4\left(-12u_x^{(m,n)} + 4u_x^{(m+1,n)} + 4u_x^{(m-1,n)} + u_x^{(m+1,n+1)} + u_x^{(m+1,n-1)} + \right. \tag{2}$$
$$\left. + u_x^{(m-1,n+1)} + u_x^{(m-1,n-1)} + u_y^{(m+1,n+1)} + u_y^{(m-1,n-1)} - u_y^{(m+1,n-1)} - u_y^{(m-1,n+1)}\right),$$

$$M\mathrm{d}_{tt}u_y^{(m,n)} = \kappa/4\left(-12u_y^{(m,n)} + 4u_y^{(m,n+1)} + 4u_y^{(m,n-1)} + u_y^{(m+1,n+1)} + u_y^{(m+1,n-1)} + \right.$$
$$\left. + u_y^{(m-1,n+1)} + u_y^{(m-1,n-1)} - u_x^{(m+1,n-1)} - u_x^{(m-1,n+1)} + u_x^{(m+1,n+1)} + u_x^{(m-1,n-1)}\right).$$

Here $u_x^{(m,n)}(t)$, $u_y^{(m,n)}(t)$ are the displacements of the cell with the coordinates (md, nd).

The mass of the boundary element is taken as a half of the mass of the inner cell and the stiffness of the axial springs at a boundary is taken as $\kappa/2$ (see the right part of Figure 2). The forces F_x^m, F_y^m act on the masses at the interface from the continuum. The equations of motion for the boundary cell read

$$\frac{1}{2}M\mathrm{d}_{tt}u_x^{(m,0)} = -\kappa/4\left(6u_x^{(m,0)} - 2u_x^{(m+1,0)} - 2u_x^{(m-1,0)} + u_y^{(m+1,-1)} - u_x^{(m+1,-1)} - \right.$$
$$\left. - u_x^{(m-1,-1)} - u_y^{(m-1,-1)}\right) - F_x^m, \tag{3}$$
$$\frac{1}{2}M\mathrm{d}_{tt}u_y^{(m,0)} = -\kappa/4\left(6u_y^{(m,0)} - 4u_y^{(m,-1)} - u_y^{(m+1,-1)} + u_x^{(m+1,-1)} - u_y^{(m-1,-1)} - \right.$$
$$\left. - u_x^{(m-1,n-1)}\right) - F_y^m.$$

We consider first a plane longitudinal incident wave that propagates towards the continuum domain with the angle of incidence $\theta = \theta_0$. Then we have two reflected waves, namely the longitudinal and transversal ones (see the right part of Figure 1). We introduce the indexes I, L and T for the incident, longitudinal and transversal waves. Then the displacements in the lattice read

$$u_x^{(m,n)} = e^{\mathrm{i}\omega\mathrm{t}}\left(A_I e^{-\mathrm{i}(mK_x^I + nK_y^I)} + A_L e^{-\mathrm{i}(mK_x^L - nK_y^L)} + A_T e^{-\mathrm{i}(mK_x^T - nK_y^T)}\right), \tag{4}$$
$$u_y^{(m,n)} = e^{\mathrm{i}\omega t}\left(B_I e^{-\mathrm{i}(mK_x^I + nK_y^I)} - B_L e^{-\mathrm{i}(mK_x^L - nK_y^L)} - B_T e^{-\mathrm{i}(mK_x^T - nK_y^T)}\right),$$

where $K_x^I = k_0 \sin\theta_0$, k_0 is a dimensionless wavenumber of the longitudinal waves (wavenumber mupltiplied by d, hereafter we will work with dimensionless wavenumbers), and according to the Snell's law $K_x^I = K_x^L = K_x^T = K_x$. The angle of reflection of longitudinal waves is then the same as the angle of incidence and $K_y^I = K_y^L = k_0 \cos\theta_0$. We denote the angle of reflection of transversal waves as $\theta = \theta_2$ and wavenumber $k = k_2$. Then $K_x^T = k_2 \sin\theta_2$, $K_y^T = k_2 \cos\theta_2$.

The wavenumber k_0 can be found numerically from the dispersion relation [1] for longitudinal waves:

$$4\cos(k_0 \sin\theta_0)\cos(k_0 \cos\theta_0) + 2\cos(k_0 \sin\theta_0) + 2\cos(k_0 \cos\theta_0) - 8 + \Omega^2 = 0, \tag{5}$$

where the angle of incidence θ_0 and the dimensionless frequency $\Omega = \omega d/c_T$ are input data, $c_T = \sqrt{\mu/\rho}$ is the shear wave velocity in the elastic continuum. As follows from the equalities (1), $\Omega^2/2 = \omega^2 M/\kappa$.

The reflection angle θ_2 and wavenumber k_2 can be found from the dispersion equation for transversal waves

$$2\cos(k_2 \sin\theta_2) + 2\cos(k_2 \cos\theta_2) - 4 + \Omega^2 = 0, \tag{6}$$

with the aid of the relation $k_2 = k_0 \sin\theta_0 / \sin\theta_2$ that follows from the Snell's law.

The dependence of the wavenumbers k_0 and k_2 on the frequency Ω for different incidence angles is depicted in Figure 2.

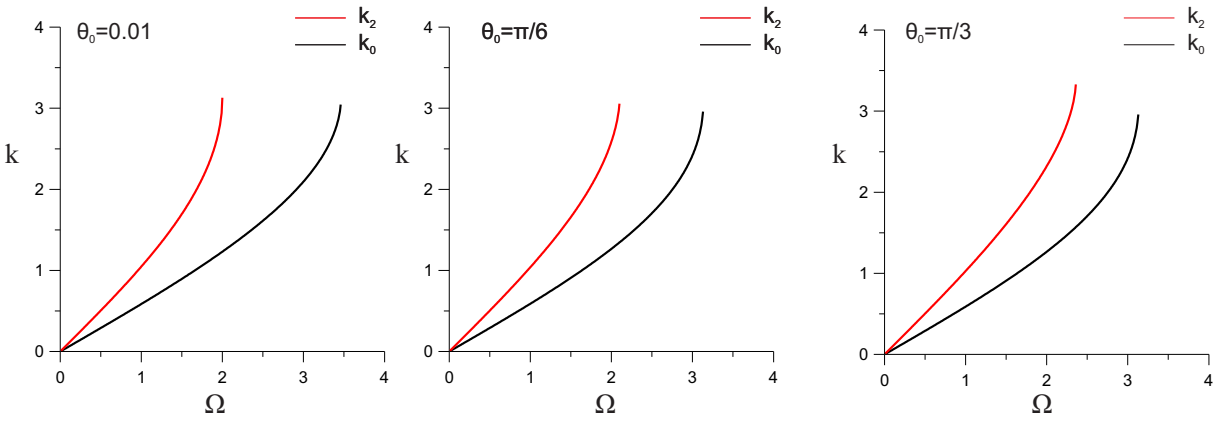

Figure 3: Wavenumbers of the longitudinal and transversal waves versus frequency for different angles of incidence

Substitution of the incident longitudinal (transversal) wave into the equations of motion (2) allows to obtain the relation between the $x-$ and $y-$components of the amplitudes of the displacements. This gives:

$$\begin{aligned} D_L &= \frac{B_I}{A_I} = \frac{B_L}{A_L} = \frac{-\Omega^2/2 + 3 - \cos(K_x)(2 + \cos(K_y^L))}{-\sin(K_x)\sin(K_y^L)}, \\ D_T &= \frac{B_T}{A_T} = \frac{-\Omega^2/2 + 3 - \cos(K_x)(2 + \cos(K_y^T))}{-\sin(K_x)\sin(K_y^T)}. \end{aligned} \tag{7}$$

In correspondence with the incident wave the forces F_x^m, F_y^m are expressed as follows:

$$F_x^m = F_x^0(\omega)exp(-imK_x)exp(\mathrm{i}\omega t), \quad F_y^m = F_y^0(\omega)exp(-imK_x)exp(\mathrm{i}\omega t). \tag{8}$$

Substitution of the displacements (4) in the equations of motion for the boundary element (3) leads to the system of two algebraic equations with four variables, namely A_L, A_T, F_x^0, F_y^0. We need two more equations to solve the system. They come from the second set of the boundary conditions that provides the continuity of displacements at the interface $y = 0$. This will be discussed in Section 4.

3 GOVERNING EQUATIONS FOR THE CONTINUUM

Equations of motion of the elastic continuum read [2]

$$\begin{aligned} \tilde{\mu}\left(\partial_{xx}u_x + \partial_{yy}u_x\right) + \left(\tilde{\lambda} + \tilde{\mu}\right)\left(\partial_{xx}u_x + \partial_{yx}u_y\right) &= \rho\partial_{tt}u_x, \\ \tilde{\mu}\left(\partial_{xx}u_y + \partial_{yy}u_y\right) + \left(\tilde{\lambda} + \tilde{\mu}\right)\left(\partial_{xy}u_x + \partial_{yy}u_y\right) &= \rho\partial_{tt}u_y, \end{aligned} \tag{9}$$

where u_x and u_y are the $x-$and $y-$ components of the vectorial displacement in the continuum. We introduce small dissipation χ: $\tilde{\lambda} = \lambda + \chi\partial_t$, $\tilde{\mu} = \mu + \chi\partial_t$. λ and μ are Lame's coefficients and $\lambda = \mu$, as it has been discussed in the previous section (1). The need to introduce a small dissipation will become clear in the course of derivation of the response of the continuum.

There is an infinite number of the points of contact between the discrete lattice and the continuum at the interface $y = 0$ (see Figure 1). At each point the forces F_x^j, F_y^j (8) act on the continuum from the lattice. We assume that there is finite contact area between each mass of the lattice and the continuum in order to avoid singularities in the solution for the classical

continuum (if this were not done, the contact forces would turn to zero). For this reason we introduce parameter b — the half-width of the contact of the continuum and one particle of the lattice at the interface. We also choose the boundary conditions such as to assure that the contact force is independent of b:

$$\int_{-b}^{b} \sigma dx = \frac{F}{h}. \tag{10}$$

Then the natural boundary conditions at the interface can be formulated:

$$\sigma_{yy}(x,0) = -\sum_{j=-\infty}^{\infty} \frac{F_y^j}{2bh} H\left(b - |x - jd|\right), \quad \sigma_{yx}(x,0) = -\sum_{j=-\infty}^{\infty} \frac{F_x^j}{2bh} H\left(b - |x - jd|\right), \tag{11}$$

where $\sigma_{yy}(x,y,t)$ is the normal stress, $\sigma_{yx}(x,y,t)$ is the shear stress, $H(x)$ is the unit step function (chosen for the sake of simplicity), j is an integer.

We also impose the correspondence between the stresses σ_{yy}, σ_{yx} and the forces F_y^j, F_x^j in the long-wave limit. This can be achieved if we take $b = d/2$.

We consider the following displacement representation:

$$u_x(x,y,t) = \partial_x \Phi(x,y,t) + \partial_y \Psi(x,y,t), \quad u_y(x,y,t) = \partial_y \Phi(x,y,t) - \partial_x \Psi(x,y,t). \tag{12}$$

Then the stresses σ_{yy} and σ_{yx} are related to the displacement potentials Φ, Ψ in the following way:

$$\sigma_{yy} = \tilde{\lambda}\left(\partial_{xx} + \partial_{yy}\right)\Phi + 2\tilde{\mu}\left(\partial_{yy}\Phi - \partial_{yx}\Psi\right), \quad \sigma_{xy} = \tilde{\mu}\left(2\partial_{xy}\Phi + \partial_{yy}\Psi - \partial_{xx}\Psi\right). \tag{13}$$

This representation satisfies the equations of motion (9) if

$$\partial_{tt}\Phi - \left(\tilde{\lambda} + 2\tilde{\mu}\right)/\rho\left(\partial_{xx} + \partial_{yy}\right)\Phi = 0, \quad \partial_{tt}\Psi - \tilde{\mu}/\rho\left(\partial_{xx} + \partial_{yy}\right)\Psi = 0. \tag{14}$$

The solutions of the above equations can be found in the form

$$\Phi(x,y,t) = \phi(x,y)e^{\mathrm{i}\omega t}, \quad \Psi(x,y,t) = \psi(x,y)e^{\mathrm{i}\omega t}. \tag{15}$$

We substitute (15) in (14) and (13) in (11), then we apply the exponential Fourier transform over the spatial coordinate y defined as

$$\phi^*(k,y) = \int_{-\infty}^{\infty} e^{\mathrm{i}kx}\phi(x,y)dx, \quad \psi^*(k,y) = \int_{-\infty}^{\infty} e^{\mathrm{i}kx}\psi(x,y)dx \tag{16}$$

and obtain the equations

$$\partial_{yy}\phi^* - \zeta_L^2\phi^* = 0, \quad \partial_{yy}\psi^* - \zeta_T^2\psi^* = 0 \tag{17}$$

with the boundary conditions at the interface $y = 0$

$$\begin{aligned}
&(\tilde{\lambda} + 2\tilde{\mu})\partial_{yy}\phi^* - \tilde{\lambda}k^2\phi^* + 2\tilde{\mu}\mathrm{i}k\partial_y\psi^* = -\sum_{j=-\infty}^{\infty} F_y^0 e^{-\mathrm{i}jdK_x}\left(e^{\mathrm{i}k(jd+b)} - e^{\mathrm{i}k(jd-b)}\right)/\mathrm{i}dhk,\\
&\tilde{\mu}\left(\partial_{yy}\psi^* + k^2\psi^* - 2\mathrm{i}k\partial_y\phi^*\right) = -\sum_{j=-\infty}^{\infty} F_x^0 e^{-\mathrm{i}jdK_x}\left(e^{\mathrm{i}k(jd+b)} - e^{\mathrm{i}k(jd-b)}\right)/\mathrm{i}dhk,
\end{aligned} \tag{18}$$

where $\zeta_L = \sqrt{k^2 - \omega^2/\tilde{c}_L^2}$, $\zeta_T = \sqrt{k^2 - \omega^2/\tilde{c}_T^2}$, $\tilde{c}_L^2 = c_L^2(1 + \mathrm{i}\chi^*)$, $\tilde{c}_T^2 = c_T^2(1 + \mathrm{i}\chi^*)$, $\chi^* = \omega\chi/\mu$; $c_L = \sqrt{(\lambda + 2\mu)/\rho}$ and $c_T = \sqrt{\mu/\rho}$ are the compressional and shear wave velocities in the classical continuum, respectively.

The general solutions of the equations (17), taking into account that the functions ϕ^*, ψ^* should have finite values when y goes to ∞, can be written in the form

$$\phi^*(k, y) = A(k, \omega)exp(-\zeta_L y), \quad \psi^*(k, y) = B(k, \omega)exp(-\zeta_T y), \tag{19}$$

provided that the real parts of the radicals ζ_L, ζ_T are assumed positive.

We find the functions $A(k, \omega)$ and $B(k, \omega)$ that satisfy the boundary conditions (18). Then we substitute (15) to (12) and apply the Fourier transform to the result in order to obtain the Fourier transforms of the displacements u_x, u_y:

$$\begin{aligned} u_x^* &= (-\mathrm{i}k\phi^* + \partial_y\psi^*) = \left(F_x^0\zeta_T(2k^2e^{-\zeta_L y} - \gamma e^{-\zeta_T y}) + F_y^0\mathrm{i}k(2\zeta_T\zeta_L e^{-\zeta_T y} - \gamma e^{-\zeta_L y})\right) S, \\ u_y^* &= (\mathrm{i}k\psi^* + \partial_y\phi^*) = \left(F_x^0\mathrm{i}k(\gamma e^{-\zeta_L y} - 2\zeta_T\zeta_L e^{-\zeta_T y}) + F_y^0\zeta_L(2k^2e^{-\zeta_T y} - \gamma e^{-\zeta_L y})\right) S, \end{aligned} \tag{20}$$

where

$$S = \frac{\sum\limits_{j=-\infty}^{\infty} e^{\mathrm{i}kjd}\left(e^{-\mathrm{i}kb} - e^{\mathrm{i}kb}\right)}{\mathrm{i}dhk\mu(1 + \mathrm{i}\chi^*)\Delta}, \quad \gamma = 2k^2 - \omega^2/\tilde{c}_T^2, \quad \Delta = \gamma^2 - 4k^2\zeta_T\zeta_L. \tag{21}$$

The inverse Fourier transform is applied to derive the displacements in the continuum according to the following relations:

$$u_x(x, y, t) = \frac{1}{2\pi}\int\limits_{-\infty}^{\infty} e^{-\mathrm{i}kx}u_x^*(x, y, t)dk, \quad u_y(x, y, t) = \frac{1}{2\pi}\int\limits_{-\infty}^{\infty} e^{-\mathrm{i}kx}u_y^*(x, y, t)dk. \tag{22}$$

4 COUPLING OF THE DOMAINS

The continuity of forces and displacements is required at the boundary $y = 0$. We have smeared the contact between the lattice and the continuum at the interface to avoid singularities in the solution for the continuum and this causes the ambiguity of the boundary problem statement.

We assume that the displacements of the masses at the boundary in the lattice are equal to the displacements of the continuum in the points of contact:

$$u_x^{(m,0,t)} = u_x(md, 0, t), \quad u_y^{(m,0,t)} = u_y(md, 0, t). \tag{23}$$

Note that one could also equate the displacements in the lattice $u_x^{(m,0,t)}$, $u_y^{(m,0,t)}$ to the displacements $u_x(md, 0, t)$, $u_y(md, 0, t)$ averaged over the width of the contact $2b$.

We substitute the displacements in the lattice (4) into (23) and apply the results of the previous section. Then the equations (23) transform to the following equations:

$$\begin{aligned} &A^{(f)}e^{-\mathrm{i}K_x m} = \int\limits_{-\infty}^{\infty} F^{(f)}e^{-\mathrm{i}kmd}\sum_{j=-\infty}^{\infty} e^{\mathrm{i}kjd}e^{-\mathrm{i}K_x j}dk, \quad f = 1, 2, \\ &A^1 = A_I + A_L + A_T, \quad A^2 = A_I D_L - A_L D_L - A_T D_T, \\ &F^1(k, \omega) = \tfrac{(2k^2-\gamma)\zeta_T F_x^0 + \mathrm{i}k(2\zeta_T\zeta_L - \gamma)F_y^0}{2\pi\mathrm{i}kdh\mu(1+\mathrm{i}\chi^*)\Delta}\left(e^{-\mathrm{i}kb} - e^{\mathrm{i}kb}\right), \\ &F^2(k, \omega) = \tfrac{-\mathrm{i}k(2\zeta_T\zeta_L - \gamma)F_x^0 + (2k^2-\gamma)\zeta_L F_y^0}{2\pi\mathrm{i}kdh\mu(1+\mathrm{i}\chi^*)\Delta}\left(e^{-\mathrm{i}kb} - e^{\mathrm{i}kb}\right). \end{aligned} \tag{24}$$

Let us multiply the left and the right parts of the equations (24) by $e^{\mathrm{i}K_x m}$ and introduce $l = j - m$. Then the equations (24) can be rewritten as follows:

$$A^{(f)} = \int\limits_{-\infty}^{\infty} F^{(f)} \sum_{l=-\infty}^{\infty} e^{\mathrm{i}l(kd-K_x)} dk. \tag{25}$$

We divide this equations by h, apply the relation $\kappa = 2\mu h$ and introduce dimensionless variables $K = kd$, $\tilde{F} = F/\kappa/h$, $b_{dl} = b/d$. After that the equations (25) take the form

$$A^1/h = C_1\tilde{F}^0_x + C_2\tilde{F}^0_y, \quad A^2/h = C_3\tilde{F}^0_x + C_4\tilde{F}^0_y, \quad C_3 = -C_2. \tag{26}$$

The coefficients C_1, C_2, C_4 should be evaluated:

$$\begin{aligned}
C_1 &= \tfrac{1}{\pi i(1+\mathrm{i}\chi^*)} \sum_{l=-\infty}^{\infty} e^{-\mathrm{i}lK_x} \int\limits_{-\infty}^{\infty} \tfrac{F_1(K,\Omega)}{K\Delta} e^{\mathrm{i}lK} \left(e^{-\mathrm{i}Kb_{dl}} - e^{\mathrm{i}Kb_{dl}}\right) dK, \\
C_2 &= \tfrac{1}{\pi i(1+\mathrm{i}\chi^*)} \sum_{l=-\infty}^{\infty} e^{-\mathrm{i}lK_x} \int\limits_{-\infty}^{\infty} \tfrac{F_2(K,\Omega)}{\Delta} e^{\mathrm{i}lK} \left(e^{-\mathrm{i}Kb_{dl}} - e^{\mathrm{i}Kb_{dl}}\right) dK, \\
C_4 &= \tfrac{1}{\pi i(1+\mathrm{i}\chi^*)} \sum_{l=-\infty}^{\infty} e^{-\mathrm{i}lK_x} \int\limits_{-\infty}^{\infty} \tfrac{F_1(K,\Omega)}{K\Delta} e^{\mathrm{i}lK} \left(e^{-\mathrm{i}Kb_{dl}} - e^{\mathrm{i}Kb_{dl}}\right) dK,
\end{aligned} \tag{27}$$

where $F_1 = \beta_T^2\sqrt{K^2-\beta_T^2}$, $F_2 = \mathrm{i}(2\sqrt{K^2-\beta_T^2}\sqrt{K^2-\beta_L^2} - 2K^2 + \beta_T^2)$, $F_4 = \beta_T^2\sqrt{K^2-\beta_L^2}$ are symmetric functions, $\beta_L^2 = \Omega^2 c_T^2/c_L^2/(1+\mathrm{i}\chi^*)$, $\beta_T^2 = \Omega^2/(1+\mathrm{i}\chi^*)$, $\Delta = (2K^2-\beta_T^2)^2 - 4K^2\sqrt{K^2-\beta_T^2}\sqrt{K^2-\beta_L^2}$.

It has been checked that the direct numerical calculation of the sums of integrals (27) is very time-consuming because one has to take a large number of the members of summation till the sum converges. To avoid this we carry out the summation analytically. We rewrite (27) in the following way:

$$\begin{aligned}
C_{1(4)} &= -\tfrac{1}{\pi\mathrm{i}(1+\mathrm{i}\chi^*)} \left(\sum_{l=1}^{\infty} \left(e^{\mathrm{i}lK_x} + e^{-\mathrm{i}lK_x}\right) \int\limits_{-\infty}^{\infty} \tfrac{F_{1(4)}(K)}{K\Delta} \left(e^{\mathrm{i}K(b_{dl}-l)} + e^{\mathrm{i}K(b_{dl}+l)}\right) dK + C_{1(4)0} \right), \\
C_2 &= -\tfrac{1}{\pi\mathrm{i}(1+\mathrm{i}\chi^*)} \sum_{l=1}^{\infty} \left(e^{\mathrm{i}lK_x} - e^{-\mathrm{i}lK_x}\right) \int\limits_{-\infty}^{\infty} \tfrac{F_2(K)}{\Delta} \left(e^{\mathrm{i}K(b_{dl}+l)} - e^{\mathrm{i}K(b_{dl}-l)}\right) dK, \\
C_{1(4)0} &= \int\limits_{-\infty}^{\infty} \tfrac{F_{1(4)}(K)}{K\Delta} \left(e^{\mathrm{i}Kb_{dl}} - e^{-\mathrm{i}Kb_{dl}}\right) dK = 2\int\limits_{-\infty}^{\infty} F_{1(4)(K)} \tfrac{e^{\mathrm{i}Kb_{dl}}-1}{K\Delta} dK.
\end{aligned} \tag{28}$$

The integrands in (28) are multiple-valued functions because of the presence of the radicals. They become infinite at so-called Rayleigh poles which are the simple zeros of the equation $\Delta(K) = 0$. This equation in the case of zero damping has been examined by Achenbach [2]. There are two real roots: $K = \pm\omega d/c_R = \Omega c_T/c_R$, where c_R is the velocity of the Rayleigh waves. With non-zero damping the roots move to the lower and upper half-planes of the complex plane: $K = \pm\beta_R$, $\beta_R = \Omega c_T/c_R/(1+\mathrm{i}\mu_{dl})$. The branch points are $K = \pm\beta_L$, $K = \pm\beta_T$. We apply the contour integration around the poles in order to evaluate the following integrals from (28):

$$\begin{aligned}
&J^1_{1(4)} = \int\limits_{-\infty}^{\infty} \tfrac{F_{1(4)}(K)}{K\Delta} e^{\mathrm{i}K(b_{dl}+l)} dK, \quad J^2_{1(4)} = \int\limits_{-\infty}^{\infty} \tfrac{F_{1(4)}(K)}{K\Delta} e^{\mathrm{i}K(b_{dl}-l)} dK, \\
&J^1_2 = \int\limits_{-\infty}^{\infty} \tfrac{F_2(K)}{\Delta} e^{\mathrm{i}K(b_{dl}+l)} dK, \quad J^2_2 = \int\limits_{-\infty}^{\infty} \tfrac{F_2(K)}{\Delta} e^{\mathrm{i}K(b_{dl}-l)} dK, \quad J_0 = \int\limits_{-\infty}^{\infty} F_{1(4)}(K) \tfrac{e^{\mathrm{i}Kb_{dl}}-1}{K\Delta} dK.
\end{aligned} \tag{29}$$

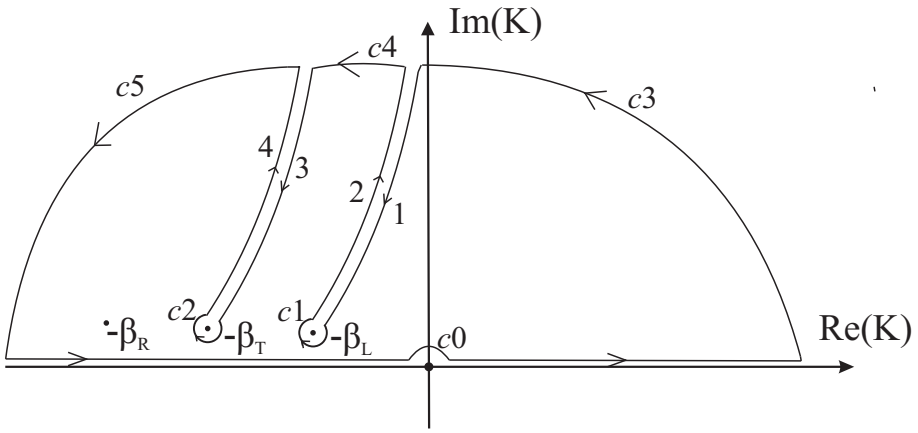

Figure 4: Contour of integration in the upper half-plane

The contour of integration and location of singular points for $J^1_{1(4)}$ are depicted in Figure 4. The contour for J^1_2 and J_0 is quite the same with the only exception that these integrals do not have a pole at $K = 0$. We integrate $J^2_{1(4)}$ and J^2_2 along the contour in the lower half-plane. The integration along the circular contours $c1$, $c2$ around the branch points vanishes as their radius decreases, the integration along the circular contours $c3$, $c4$, $c5$ vanishes as $|K| \to \infty$. Thus,

$$\oint f(K)dK = \left(\int\limits_{c0} + \int\limits_{1} + \int\limits_{2} + \int\limits_{3} + \int\limits_{4} + \int\limits_{-\infty}^{\infty} \right) f(K)dK = 2\pi \mathrm{i} \mathrm{Res}\left[f(K), K = -\beta_R \right], \quad (30)$$

where $\int\limits_{-\infty}^{\infty}$ is to be understood in the sense of Cauchy principal value. The pole $K = 0$ was artificially introduced as the original integrals $C_{1(4)}$ from (27) do not have this pole. In accordance with this fact the integrals around the circular contour $c0$ in the upper and in the lower half-planes have the same absolute value but are of the opposite sign and thus vanish in the sum $J^1_{1(4)} + J^2_{1(4)}$.

$\mathrm{Im}(\sqrt{K^2 - \beta_L^2}) = 0$ on the contours of integration 1–2 and $\mathrm{Im}(\sqrt{K^2 - \beta_T^2}) = 0$ on the contours of integration 3–4. These equalities hold true if $2\mathrm{Im}(K)\mathrm{Re}K = \alpha_i$, $i = 1, 2$, where $\alpha_1 = \mathrm{Im}(\beta_L^2) = -\Omega^2 \chi^* c_T^2 / c_L^2 / (1 + \chi^{*2})$, $\alpha_2 = \mathrm{Im}(\beta_T^2) = -\Omega^2 \chi^* / (1 + \chi^{*2})$. The general representation of K at the contours 1–4 is $K = a + i\alpha/2/a$, where $a = \mathrm{Re}(K)$ and $\alpha = \alpha_1$ or α_2 are negative. Thus $|exp(\mathrm{i}lK)| = |exp(-\alpha/2/a)| < 1$. Now we swap the order of summation and integration and evaluate the sums from (28) as the sums of geometric progression:

$$\sum_{l=1}^{\infty} \left(e^{\mathrm{i}lK_x} \pm e^{-\mathrm{i}lK_x} \right) e^{\mathrm{i}lK} = \frac{e^{\mathrm{i}(K_x+K)}}{1 - e^{\mathrm{i}(K_x+K)}} \pm \frac{e^{\mathrm{i}(K-K_x)}}{1 - e^{\mathrm{i}(K-K_x)}}. \quad (31)$$

In the lower half-plane we have K with the opposite sign, $|exp(-ilK)| < 1$ and we can apply the formulae of the sum of geometric progression as well.

The evaluation accomplished in Eq (31) would have been impossible if no damping were present in the continuum. that is why it has been introduced in Section 3.

5 THE REFLECTION COEFFICIENTS

The amplitude reflection coefficient is found as the absolute value of the ratio of the complex amplitudes of reflected and incident waves and is given as $R_L = |A_L/A_I|$ for longitudinal wave

and as $R_T = |A_T/A_I|$ for transversal wave. These coefficients can be found by solving the system of four linear equations that constitute the boundary conditions. We substitute (4) and (8) into (3) and divide the whole equations by κA_I. Then we take the equations (26) and divide them by A_I/h. Finally, we have the system of four equations:

$$\begin{cases} a_{11}\tilde{A}_L + a_{12}\tilde{A}_T + \tilde{\tilde{F}}_x = b_1, & a_{21}\tilde{A}_L + a_{22}\tilde{A}_T + \tilde{\tilde{F}}_y = b_2, \\ \tilde{A}_L + \tilde{A}_T - C_1\tilde{\tilde{F}}_x - C_2\tilde{\tilde{F}}_y = -1, & \tilde{A}_L D_L + \tilde{A}_T D_T + C_3\tilde{\tilde{F}}_x + C_4\tilde{\tilde{F}}_y = D_L, \end{cases} \tag{32}$$

where $\tilde{A}_{L(T)} = A_{L(T)}/A_I$, $\tilde{\tilde{F}}_{x(y)} = F^0_{x(y)}/\kappa/A_I$ are the unknowns and

$$\begin{aligned} a_{11} &= -\cos(K_x) - 0.25\Omega^2 + 1.5 + 0.5\exp(\mathrm{i}K_y^L)(\mathrm{i}D_L\sin(K_x) - \cos(K_x)), \\ a_{12} &= -\cos(K_x) - 0.25\Omega^2 + 1.5 + 0.5\exp(-\mathrm{i}K_y^T)(\mathrm{i}D_T\sin(K_x) - \cos(K_x)), \\ a_{21} &= D_L(0.25\Omega^2 - 1.5 + \exp(-\mathrm{i}K_y^L)) + 0.5\exp(-\mathrm{i}K_y^L)(D_L\cos(K_x) - \mathrm{i}\sin(K_x)), \\ a_{22} &= D_T(0.25\Omega^2 - 1.5 + \exp(-\mathrm{i}K_y^L)) + 0.5\exp(-\mathrm{i}K_y^L)(D_T\cos(K_x) - \mathrm{i}\sin(K_x)), \\ b_1 &= \cos(K_x) + 0.25\Omega^2 - 1.5 + 0.5\exp(\mathrm{i}K_y^L)(\mathrm{i}D_L\sin(K_x) + \cos(K_x)), \\ b_2 &= D_L(0.25\Omega^2 - 1.5\exp(\mathrm{i}K_y^L)) + 0.5\exp(\mathrm{i}K_y^L)(D^L\cos(K_x) + \mathrm{i}\sin(K_x)). \end{aligned} \tag{33}$$

The input data for the system (32) includes the angle of incidence θ_0 and the dimensionless frequency Ω. The admissible values of θ_0 are between 0 and $\pi/2$ and that of Ω are between 0 and the cut-off frequency Ω_c up to which the longitudinal waves propagate.

We consider the flux of energy through the remote area in the lattice parallel to the interface. The flux of the wave energy is proportional to the square of its amplitude. The energy reflection coefficient is found as the ratio of the energy fluxes of reflected and incident waves and is given as $P_L = R_L^2$ and $P_T = \xi R_T^2$, where

$$\xi = \frac{4D_T^2\sin(K_y^T) + \sin(K_x + K_y^T)(2D_T + D_T^2 + 1)\sin(K_x - K_y^T)(2D_T - D_T^2 - 1)}{4D_L^2\sin(K_y^L)\sin(K_x + K_y^L)(2D_L + D_L^2 + 1) + \sin(K_y^L - K_x)(1 + D_L^2 - 2D_L)}. \tag{34}$$

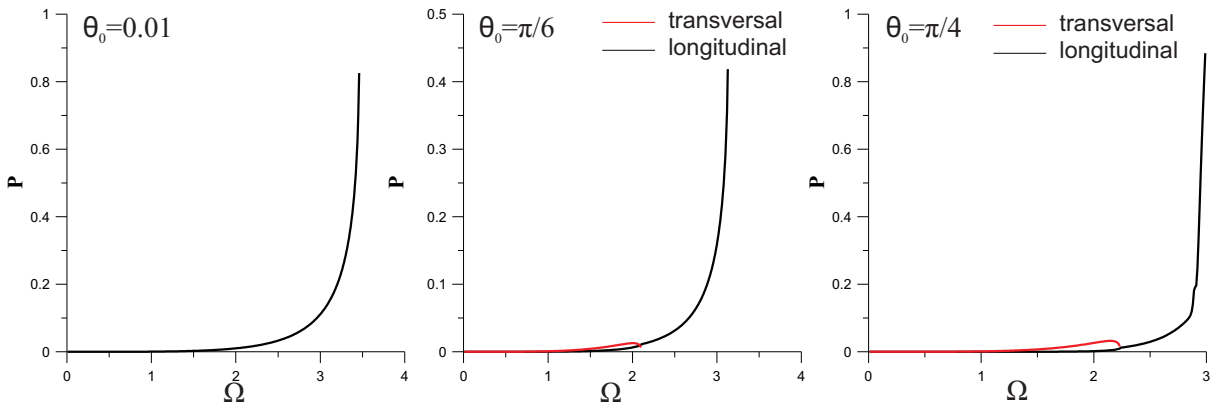

Figure 5: The energy reflection coefficients for different angles of incidence

To demonstrate the results the following parameters for the continuum are taken: $\rho = 2300$ kg/m^3, $E = 230$ GPa. As coefficient $\mu = 0.5E/(1+\nu)$ should be equal to $\lambda = \nu E/(1+\nu)(1-2\nu)$, the Poisson's ratio of the continuum is $\nu = 0.25$. The damping parameter μ^*=1000 Pa·sec. The period of the lattice $d = 0.05$ m. The values of the parameter $\mu_{dl} = \omega\mu^*/\mu = \Omega c_T \mu^*/d/\mu$ lie between 0 and 0.02 depending on the frequency Ω.

The dependence of the energy reflection coefficient P (either P_L or P_T) on the dimensionless frequency Ω for three different angles of incidence is depicted in Figure 5. One can see that there is almost no reflection at low frequencies, where the continuum is capable of approximating the lattice, and at higher frequencies the reflection grows rapidly as the dispersion properties of the lattice and the continuum differ a lot. One can also note that the reflection of transversal wave is less than that of the longitudinal one.The graph of P_T stops at a lower frequency than that of P_L as the cut-off frequency of the transversal waves is lower than that of the longitudinal waves.

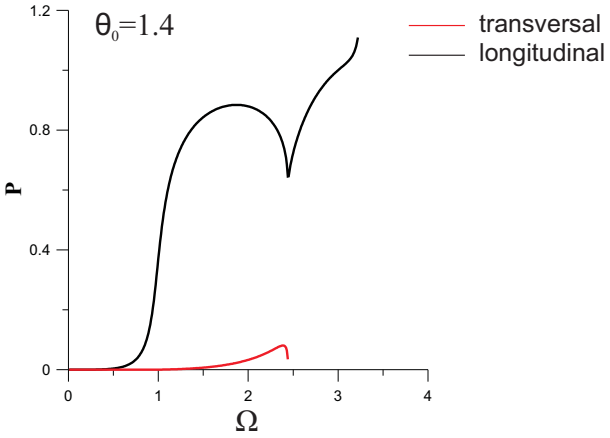

Figure 6: The energy reflection coefficient

For the angles of incidence that are larger than $\pi/4$ we have obtained non-physical results: the reflected energy exceeds the energy of the incident wave. This anomalous reflection is depicted in Figure 6. We do not yet know the genuine explanation of this result. Most likely, it is a consequence of the boundary conditions at the interface.

The case when transversal wave falls on the interface from the lattice has also been examined. The energy reflection coefficients for different angles of incidence are depicted in Figure 7.

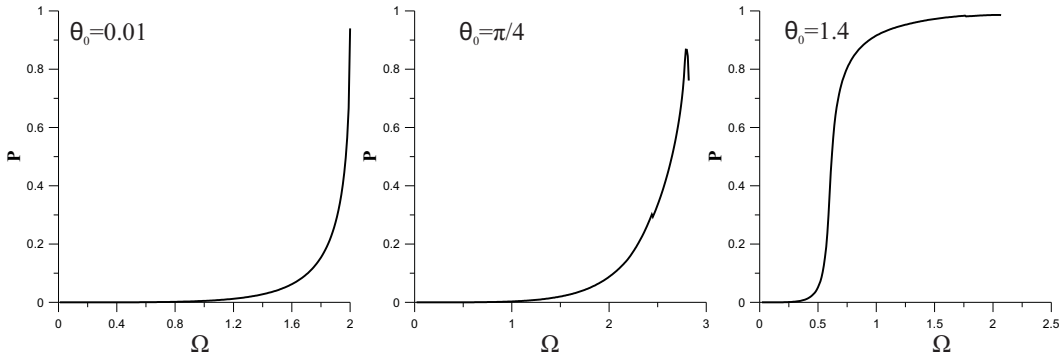

Figure 7: The energy reflection coefficients for different angles of incidence

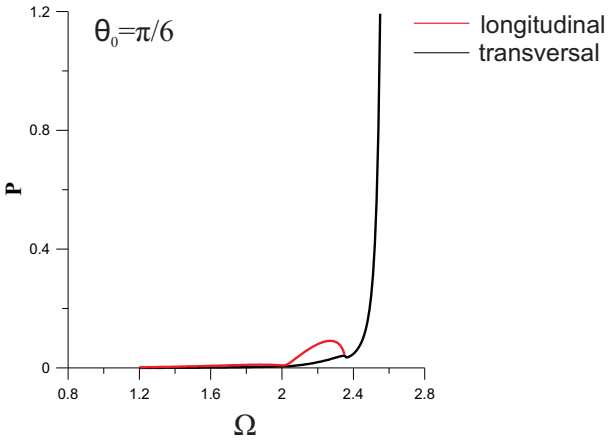

Figure 8: The energy reflection coefficient

The reflection of the longitudinal waves is negligible when $\theta_0 = 0.01$. In the cases $\theta_0 = \pi/4$ and $\theta_0 = 1.4$ the longitudinal waves do not reflect.

The anomalous reflection has also been observed in this case (see Figure 8).

6 CONCLUSIONS

The motivation for this study has been to facilitate the development of the multi-scale numerical approaches that are becoming increasingly popular in investigations into the details of dynamic deformations of various materials. Specifically, this paper is envisaged to be of interest for those researchers who employ the discrete-continuum models in order to minimize the huge computational costs associated with the detailed discrete modelling. The continuum domain in such models is introduced in order to minimize the size of the discrete domain as much as possible thereby significantly reducing the computation time. To achieve this, however, the continuum domain should not introduce spurious reflections at as broad as possible frequency range. In this paper, the capabilities of the classical continuum have been assessed to comply with this requirement. To this end, the reflection of plane harmonic waves at the interface of the square lattice and the classical continuum has been studied. A method has been proposed to couple the domains in such a manner that no singularities occur due to the point-like character of particles in the lattice. It has been shown that while the classical continuum can serve as a non-reflecting boundary for the lattice at low frequencies, it cannot absorb higher frequency waves. Moreover, it has been found that due to the ambiguity in the formulation of the boundary conditions at the discrete-continuum interface, the energy of the reflected waves can be mathematically predicted in some cases to be larger that that of the incident waves — a result that is physically unacceptable. Given the above-formulated results, it can be concluded that the classical continuum is not the most desirable model for assuring the non-reflective conditions at a wide frequency band. One of the attractive alternatives could be a gradient continuum that, according to a recent study carried out in the 1D framework [9], can be expected to match the lattice at a wide frequency band. Additionally, no singularities occur at the contact between a point load and a surface of a gradient continuum. The authors of this contribution are currently investigating whether gradient continua will be up to these expectations in the multidimensional case.

REFERENCES

[1] A.S.J. Suiker, A.V. Metrikine, R. De Borst, Dynamic behaviour of a layer of discrete particles, part 1: analysis of body waves and eigenmodes. *Journal of Sound and Vibration*, **240(1)**, 1 – 18, 2001.

[2] J.D. Achenbach, Wave propagation in elastic solids. *North-Holland Publishing Company, Amsterdam-London*, 425p, 1973.

[3] R.E. Rudd, J.Q. Broughton, Coarse-grained molecular dynamics and the atomic limit of finite elements. *Phys. Rev. B* **58**, R5893 – 6, 1998.

[4] W. Cai, M.D. Koning, V.V. Bulatov, S.Yip, Minimizing boundary reflections in coupled-domain simulations. *Phys. Rev. Lett.* **85**, 3213 – 16, 2000.

[5] E.G. Karpov, G.J. Wagner, W.K. Liu, A Greens function approach to deriving non-reflecting boundary conditions. *Int. J. Numer. Meth. Engng* **62**, 1250 – 1262, 2005.

[6] W. E, Z. Huang, Matching conditions in atomistic-continuum modeling of materials. *Phys. Rev. Lett.* **87**, 135501, 2001.

[7] Wagner, Liu, Coupling of atomistic and continuum simulations using a bridging scale decomposition. *Journal of Computational Physics* **190**, 249 – 274, 2003

[8] S.P. Xiao, T. Belytschko, A bridging domain method for coupling continua with molecular dynamics. *Comput. Methods Appl. Mech. Engrg.*, **193**, 1645 – 1669, 2004

[9] A.M. Kudarova, A.V. Metrikine, On the use of gradient continua for minimizing the wave reflection at a discrete-continuum interface. *Proceedings of XXXVIII International summer school-conference APM'2010*, 383 – 390, 2010.